Dynamic Model of Hip and Ankle Joints Loading during Working with a Motorized Backpack Sprayer

S. Karimi Avargani[1], A. Maleki[2*], Sh. Besharati[3], R. Ebrahimi[4]

1- M.Sc. Student of Mechanical Engineering of Biosystems Department, Faculty of Agriculture, Shahrekord University, Shahrekord, Iran

2- Associate Professor of Mechanical Engineering of Biosystems Department, Faculty of Agriculture, Shahrekord University, Shahrekord, Iran

3- Lecture of Mechanical Engineering of Biosystems Department, Faculty of Agriculture, Shahrekord University, Shahrekord, Iran

4- Assistant Professor, Mechanical Engineering, Faculty of Engineering, Yasouj University, Yasouj, Iran

(*- Corresponding Author Email: maleki@sku.ac.ir)

Abstract

The main objective of this paper is to develop a seven-link dynamic model of the operator's body while working with a motorized backpack sprayer. This model includes the coordinates of the sprayer relative to the body, the rotational inertia of the sprayer, the muscle moments acting on the joints, and a kinematic coupling that keeps the body balanced between the two legs. The constraint functions were determined and the non-linear differential equations of motion were derived using Lagrangian equations. The results show that undesirable fluctuations in the ankle force are noticeable at the beginning and end of a swing phase. Therefore, injuries to the ankle joint are more likely due to vibrations. The effects of engine speed and sprayer mass on the hip and ankle joint forces were then investigated. It is found that the engine speed and sprayer mass have significant effects on the hip and ankle forces and can be used as effective control parameters. The results of the analysis also show that increasing the engine speed increases the frequency of the hip joint force. However, no significant effects on the frequency of the ankle joint force are observed. The results of this study may provide researchers with insight into estimating the allowable working hours with the motorized backpack sprayers, prosthesis design, and load calculations of hip implants in the future.

Keywords: Lagrange equation, Operator, Vibration, Weight of sprayer

Introduction

One of the most popular ways of crop protection against weeds and pests is applying motorized backpack sprayers. The use of the motorized backpack sprayer eliminates the need for hand pumping and is suitable for small-scale farms. However, the major disadvantage of motorized backpack sprayers is the external forces acting on the operator's body (Kouchakzadeh, & Beigzadeh, 2015).

Forces acting on the human body are important factors in the initiation and progression of joint disease (Astephen, Deluzio, Caldwell, & Dunbar, 2008). Force analysis of hip and ankle joints can be useful in the development of strategies to avoid and manage conditions such as osteoarthritis and deterioration of femoroacetabular (Correa, Crossley, Kim, & Pandy, 2010). Force analysis of hip and ankle joints requires multi-segment models.

Several researches have been done on the dynamic modeling of the human body. Kuo (2001) applied a simple model of bipedal walking to evaluate simple hypotheses for the metabolic cost of muscle activity. Tlalolini, Chevallereau, & Aoustin (2010) optimized the walking motions of a bipedal model by minimizing the value of the torque. The optimization process was carried out with and without the rotation of the supporting foot about the toe. Huang, Wang, Chen, Xie, & Wang (2012) employed a seven-link dynamic bipedal walking model with flat feet to analyze the dynamics of walking. The results indicated that ankle stiffness plays different roles in different gaits. Martin & Schmiedeler (2014) proposed four and six link planar biped models with knees and rigid circular feet; The ankle was not considered in the four link model. The results showed that the model with ankles is more accurate in predicting energy consumption during normal human walking at different speeds. Sharbafi & Seyfarth (2015) utilized a five link model with a rigid upper body and two segmented legs to extract internal relations between the joints' angles and stance leg orientation which hold the configuration harmonized during the gaits. Jena, Kumar, Singh, & Mani (2016) developed a biomechanical model to predict metabolic energy consumption for carrying load manually by varying modes (head, shoulder, and back), loads, and ground inclinations. The results indicated that frontal torque (in shoulder mode) requires higher physiological energy than sagittal torque. Ma, Xu, Fang, Lv, & Zhang (2022) present the dynamic model of the human-prosthesis heterogeneous coupled system. Ma, Xu, & Zhang (2023) also applied control strategies for prosthesis walking on stochastically uneven terrain.

Mechanical actions of muscles are necessary for dynamical modeling of the human body and can be considered as moments applied at the joints. Weiss, Kearney, & Hunter (1986) indicated that the moment–angle relationships in the hip, knee, and ankle joints are similar to that of a non-linear spring. Maletsky & Hillberry (2005) designed a dynamic knee simulator to reproduce the loading and kinematics of the human knee during different activities. Lim & Park (2018) developed a model for human locomotion with a curvy foot connected to a leg by a springy segment. Thus, the oscillations of the center of mass during walking can be described by the mechanics of a simple passive Spring Loaded Inverted Pendulum (SLIP). Kim, Lee, & Koo (2018) simulated joint reaction forces, active moments by muscles, and passive moments by connective tissues. They found that, at Chopart and Lisfranc joints, passive moments were responsible for large portions of the net moment. The passive structures and passive moments in the midfoot joints provide strength and prevent injuries.

Carrying backpack loads for long distances is common in a range of human activities. As a result, the influence of backpack carriage on physical performance has been investigated to establish guidelines for safe load limits. Liu (2007) analyzed the effect of backpack load position, walking speed, and surface grade on the physiological responses of infantry soldiers. The results confirmed that positioning the backpack mass center as near as possible to the body mass center resulted in the lowest energy consumption. Alamoudi, Travascio, Onar-Thomas, Eltoukhy, & Asfour (2018) determined the effect of different carrying methods on walking stability using motion capture analysis. The results confirmed that the lack of stability in the frontal carriage forced the body to increase the cadence to maintain stability. Additionally, to minimize the moment generated by both the upper body and the heavy load, participants tended to decrease the length of their stride. Walsh, Low, & Arkesteijn (2018) studied the effect of stable and unstable load carriage on walking gait variability, dynamic stability, and muscle activity of older adults. The results showed that unstable load carriage reduces dynamic stability compared to unloaded walking.

Reviewing the literature reveals that the investigation of the joint forces during load carrying is important for preventing joint injuries. However, to date, no research has

been published on the joint forces during the working with the motorized backpack sprayers. Therefore, the initial objective of the present study is to develop a seven-link dynamic model of the operator's body while working with a motorized backpack sprayer. The secondary goal of this research is to examine the effects of different working conditions (engine speed and mass of sprayer) on the hip and ankle joint forces. This is a continuation of our previous work, where the torque–angle relationships in the hip, knee, and ankle joints for the backpack sprayer operator body were discussed (Karimi Avargani, Maleki, Besharati, & Ebrahimi, 2020).

Materials and Methods

In this section, the principle of the Lagrange equation for nonholonomic constraints is introduced. The total kinetic energy, potential energy, generalized forces, and constraints are expressed for the proposed model. The non-linear equations of motion are formulated using Lagrangian equations and solved using Maple software (Ver 2015).

Lagrange Equation for Nonholonomic Constraints

Lagrangian equations have a special place in analytical mechanics. They represent equations of motion in terms of generalized coordinates. A holonomic constraint in the system of n generalized coordinates q_i can be written as Eq. 1.

$$g_j(q_1, q_2, ..., q_n, t) = 0 \qquad (1)$$

For nonholonomic constraints, Eq. 1 changes into a differential form in Eq. 2 (D'Souza & Garg, 1984; Greenwood, 1988):

$$\sum_{\upsilon=1}^{n} a_{l\upsilon} dq_{\upsilon} + a_{lt} dt = 0 \qquad l=1, 2, ... , s \qquad (2)$$

Where $\upsilon=1, 2, ..., n$ and $l=1, 2, ..., s$ are the number of coordinates and number of constraints, respectively ($n>s$). Eq. 3 expresses Lagrange's equation for constrained systems.

$$\frac{d}{dt}\left(\frac{\partial T}{\partial \dot{q}_{\upsilon}}\right) - \frac{\partial T}{\partial q_{\upsilon}} + \frac{\partial V}{\partial q_{\upsilon}} - \sum_{l=1}^{s} \lambda_l a_{l\upsilon} = Q_{\upsilon} \qquad \upsilon=1, 2, ..., n \qquad (3)$$

Where T, V, λ_l, and Q_v are kinetic energy, potential energy, Lagrange's coefficients, and generalized force related to generalized coordinate q_i, respectively. These n equations have $n+s$ unknowns, namely the n coordinates (q_v) and the s Lagrange multipliers (λ_l). The additional equations (Eq. 2) are needed for the s constraint which is coupled with the q_v. However, as shown in Eq. 4, these are considered as differential equations.

$$\sum_{\upsilon=1}^{n} a_{l\upsilon} \dot{q}_{\upsilon} + a_{lt} = 0 \qquad l=1, 2, ..., s \qquad (4)$$

Dynamic model of operator's body during spraying

Fig. 1 shows the proposed dynamical model of the operator's body during working with a motorized backpack sprayer. This model includes two rigid legs connected to the rigid upper body with hinges at the hips. Each leg includes the thigh, shank, and foot. The thigh and the shank are connected at the knee joint and the foot and the shank are connected at the ankle joint. A point mass m_h at the hip represents the pelvis. The mass of upper body m_b, leg m_l, thigh m_t, shank m_s, and foot m_f are considered lumped parameters. Longitudinal parameters c_b, c_f, c_l, c_s, c_t, l, l_s, and l_t are distances from the hip joint to the Center of Mass (CoM) of upper body, from the ankle joint to CoM of foot, from the hip joint to CoM of stance leg, from knee joint to CoM of shank, from the hip joint to CoM of thigh, stance leg length, shank length, and thigh length, respectively. The motorized backpack sprayer is located at position (x_{sp}, y_{sp}) from the CoM of the upper body.
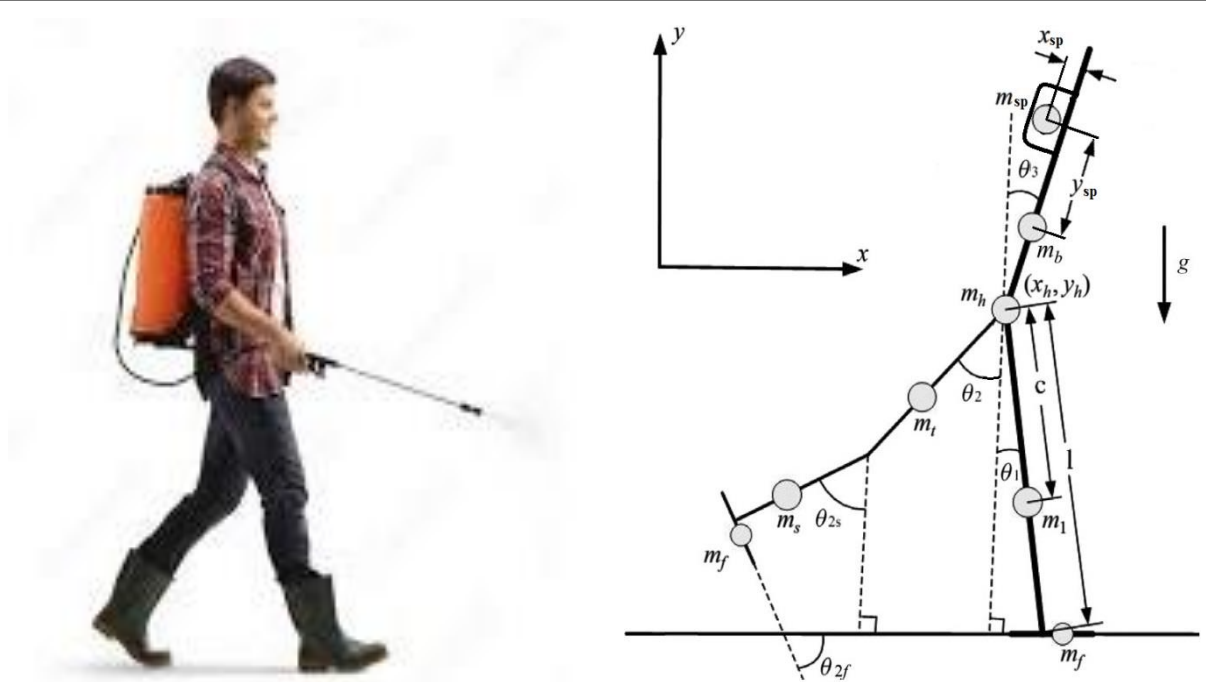
Fig.1. The proposed dynamical model of the operator's body while working with a motorized backpack sprayer

The total kinetic energy, potential energy, generalized forces, and constraints are expressed using the following assumptions (Wisse, Schwab, & van der Helm, 2004):

- The joints have no damping or friction.
- Bones do not suffer from flexible deformation.
- A kinematic coupling has been used in the model to keep the body midway between the two legs.
- The shank of the foot stance is always locked and the whole leg can be modeled as one rigid stick.
- There is enough friction between the walker and the ground. Thus, a flat foot does not deform or slip.
- The muscle moments acting on the hip, knee, and ankle joints are modeled as non-linear torsional springs.
- The sprayer engine is an unbalanced force. This can be caused by the deposition or erosion of the rotational parts.

Kinetic Energy

As shown in Fig. 1, it is assumed that the x-axis is along the ground while the y-axis is vertical to the ground pointing upward. The dynamic model for the operator's body while working with a motorized backpack sprayer can be described by the generalized coordinates (Eq. 5).

$$q^T = [x_h, y_h, \theta_1, \theta_2, \theta_3, \theta_{2s}, \theta_{2f}] \qquad (5)$$

Where x_h, y_h, θ_1, θ_2, θ_3, θ_{2s}, and θ_{2f} are the horizontal coordinate of hip joint, vertical coordinate of hip joint, the angle between vertical axis and the stance leg, the swing angle between vertical axis and the thigh, the angle between vertical axis and the upper body, the swing angle between vertical axis, and the shank and the angle between horizontal axis and foot, respectively. The positive direction of all the angles is counterclockwise. The total kinetic energy of the system is defined as the sum of the kinetic energy of the point masses, and the translational and rotational kinetic energy of the motorized backpack sprayer. The expression for the kinetic energy is obtained in Eq. 6.

$$T = T_h + T_l + T_t + T_b + T_{sp} + T_s + T_f$$
$$= \frac{1}{2}[m_h + m_l + m_t + m_b + m_{sp} + m_s + m_f]\dot{x}_h^2$$
$$+ \frac{1}{2}[m_h + m_l + m_t + m_b + m_{sp} + m_s + m_f]\dot{y}_h^2$$
$$+ \frac{1}{2}m_l c_l^2 \dot{\theta}_1^2 + \frac{1}{2}[m_t c_t^2 + m_s l_t^2 + m_f l_t^2]\dot{\theta}_2^2$$
$$+ \frac{1}{2}[I_{sp} + m_b c_b^2 + m_{sp}[(c_b + y_{sp})^2 + x_{sp}^2]]\dot{\theta}_3^2$$
$$+ \frac{1}{2}[m_s c_s^2 + m_f l_s^2]\dot{\theta}_{2s}^2 + \frac{1}{2}m_f c_f^2 \dot{\theta}_{2f}^2 + m_l c_l \dot{\theta}_1(\dot{x}_h \cos\theta_1 + \dot{y}_h \sin\theta_1)$$
$$- m_t c_t \dot{\theta}_2(\dot{x}_h \cos\theta_2 - \dot{y}_h \sin\theta_2) + m_b c_b \dot{\theta}_3(\dot{x}_h \cos\theta_3 - \dot{y}_h \sin\theta_3)$$
$$+ m_{sp}\dot{\theta}_3\{[(c_b + y_{sp})\dot{x}_h + x_{sp}\dot{y}_h]\cos\theta_3 + [x_{sp}\dot{x}_h - (c_b + y_{sp})\dot{y}_h]\sin\theta_3\}$$

$$+ m_s\{l_t c_s \dot{\theta}_2 \dot{\theta}_{2s}\cos(\theta_2 - \theta_{2s}) - \dot{x}_h[l_t \dot{\theta}_2 \cos\theta_2 + c_s \dot{\theta}_{2s}\cos\theta_{2s}] + \dot{y}_h[l_t \dot{\theta}_2 \sin\theta_2 + c_s \dot{\theta}_{2s}\sin\theta_{2s}]\}$$
$$+ m_f\{l_t l_s \dot{\theta}_2 \dot{\theta}_{2s}\cos(\theta_2 - \theta_{2s}) + c_f l_t \dot{\theta}_2 \dot{\theta}_{2f}\sin(\theta_{2f} - \theta_2) + c_f l_s \dot{\theta}_{2s} \dot{\theta}_{2f}\sin(\theta_{2f} - \theta_{2s})$$
$$- \dot{x}_h[l_t \dot{\theta}_2 \cos\theta_2 + l_s \dot{\theta}_{2s}\cos\theta_{2s} + c_f \dot{\theta}_{2f}\sin\theta_{2f}]$$
$$+ \dot{y}_h[l_t \dot{\theta}_2 \sin\theta_2 + l_s \dot{\theta}_{2s}\sin\theta_{2s} - c_f \dot{\theta}_{2f}\cos\theta_{2f}]\} \tag{6}$$

Where I_{sp} is the mass moment of inertia of the sprayer about its principal axis.

Potential Energy

The total potential energy of the system is given in Eq. 7 and is defined as the sum of the gravitational energy of the point masses.

$$U = U_h + U_l + U_t + U_b + U_{sp} + U_s + U_f$$
$$= -[m_h l + m_l(l - c_l) + m_t l + m_b l + m_{sp} l + m_s l]g(1 - \cos\theta_1)$$
$$+ [m_t c_t + m_s l_t]g(1 - \cos\theta_2) - [m_b c_b + m_{sp}(c_b + y_{sp})]g(1 - \cos\theta_3)$$
$$+ m_{sp} g x_{sp}\sin\theta_3 + m_s g c_s(1 - \cos\theta_{2s})$$
$$+ m_f g(l\cos\theta_1 - l_t\cos\theta_2 - l_s\cos\theta_{2s} - c_f\sin\theta_{2f}) \tag{7}$$

Generalized Forces

The generalized forces acting on the operator's body while working with a motorized backpack sprayer include forces resulting from gravity and are unbalanced due to erosion of the sprayer engine, muscle moment acting on the hip joint, muscle moment acting on the knee joint, and muscle moment acting on the ankle joint. The generalized forces Q_{qi} are given by the following equations (Eq. 8-14).

$$Q_{x_h} = m_0 e \omega^2 \cos(\omega t) \tag{8}$$

$$Q_{y_h} = m_0 e \omega^2 \sin(\omega t) \tag{9}$$

$$Q_{\theta_1} = T_{1f} \tag{10}$$

$$Q_{\theta_2} = T_2 \tag{11}$$

$$Q_{\theta_3} = m_0 e \omega^2 \cos\omega t[(c_b + y_{sp})\cos\theta_3 + x_{sp}\sin\theta_3]$$
$$+ m_0 e \omega^2 \sin\omega t[-(c_b + y_{sp})\sin\theta_3 + x_{sp}\cos\theta_3] \tag{12}$$

$$Q_{\theta_{2s}} = T_{2s} \tag{13}$$

$$Q_{\theta_{2f}} = 0 \tag{14}$$

Where m_0, e, and ω are the unbalanced mass of the sprayer engine, the unbalanced mass eccentricity, and the engine speed, respectively.

The muscle moment acting on the hip joint T_2 (the swing leg, Eq. 15), muscle moment acting on the knee joint T_{2s} (the swing leg, Eq. 16), and muscle moment acting on the ankle joint T_{1f} (stance leg, Eq. 17) are non-linear functions of the angle between the two segments (Karimi et al., 2020).

$$T_2 = 0.0007(\theta_2 - \theta_3)^3 - 0.0258(\theta_2 - \theta_3)^2 + 0.3236(\theta_2 - \theta_3) - 1.6792 \tag{15}$$

$$T_{2s} = -0.0011(\theta_{2s} - \theta_2)^2 - 0.0029(\theta_{2s} - \theta_2) + 1.2683 \tag{16}$$

$$T_{1f} = 0.0043\theta_1^3 + 0.0429\theta_1^2 + 0.5052\theta_1 + 3.1455 \tag{17}$$

Constraints

A constraint can be expressed by a relationship between generalized coordinates and time. When foot contact with the ground is maintained, first and second constraint equations can be represented as Eq. 18 and 19.

$$y_h - l\cos\theta_1 = 0 \tag{18}$$

$$x_h + l\sin\theta_1 - x_{ankle} = 0 \tag{19}$$

Here, the x_{ankle} is the fixed position of the ankle of the stance leg. In the passive dynamical model of a walking human, the upper body can be considered as an inverted pendulum jointed at the hip. Therefore, a kinematic coupling has been used in the model to keep the upper body between the two legs and achieve stable walking (Wisse et al., 2004). The equation of the kinematic coupling constraint is introduced according to Eq. 20.

$$2\theta_3 - (\theta_1 + \theta_2) = 0 \tag{20}$$

The time course of hip, knee, and ankle joint angles for the proposed model are given in Eqs. 21-23 (Karimi et al., 2020).

$$\theta_2 - \theta_3 = 373.64t^3 - 762.66t^2 + 414.86t - 38.89 \tag{21}$$

$$\theta_{2s} - \theta_2 = -6357.5t^3 + 4911.3t^2 - 958.48t + 1.24 \tag{22}$$

$$\theta_1 = 451.84t^3 - 513.31t^2 + 218.5t - 27.77 \tag{23}$$

According to Eq. 4, the constraint equations (Eqs. 18-23) can be considered in differential form, as defined in Eqs. 24-29:

$$\dot{y}_h + l\sin\theta_1 \dot{\theta}_1 = 0 \tag{24}$$

$$\dot{x}_h + l\cos\theta_1 \dot{\theta}_1 = 0 \tag{25}$$

$$\dot{\theta}_1 + \dot{\theta}_2 - 2\dot{\theta}_3 = 0 \tag{26}$$

$$\dot{\theta}_2 - \dot{\theta}_3 - 1120.92t^2 + 1525.32t - 414.86 = 0 \tag{27}$$

$$\dot{\theta}_2 - \dot{\theta}_{2s} - 19072.5t^2 + 9822.6t - 958.48 = 0 \tag{28}$$

$$\dot{\theta}_1 - 1355.52t^2 + 1026.62t - 218.5 = 0 \tag{29}$$

By applying Lagrange's equation (Eq. 3) and introducing the constant coefficients, seven coupled non-linear differential equations of motion can be obtained (Eqs. 30-36).

$$\eta_1 \ddot{x}_h + \eta_2 \cos\theta_1 \ddot{\theta}_1 - \eta_3 \cos\theta_2 \ddot{\theta}_2 + [\eta_4 \cos\theta_3 + \eta_5 \sin\theta_3]\ddot{\theta}_3 - \eta_6 \cos\theta_{2s}\ddot{\theta}_{2s}$$
$$- \eta_7 \sin\theta_{2f}\ddot{\theta}_{2f} - \eta_2 \sin\theta_1 \dot{\theta}_1^2 + \eta_3 \sin\theta_2 \dot{\theta}_2^2 - [\eta_4 \sin\theta_3 - \eta_5 \cos\theta_3]\dot{\theta}_3^2$$
$$+ \eta_6 \sin\theta_{2s}\dot{\theta}_{2s}^2 - \eta_7 \cos\theta_{2f}\dot{\theta}_{2f}^2 + \lambda_2 = m_0 e\omega^2 \cos(\omega t) \tag{30}$$

$$\eta_1 \ddot{y}_h + \eta_2 \sin\theta_1 \ddot{\theta}_1 + \eta_3 \sin\theta_2 \ddot{\theta}_2 - [\eta_4 \sin\theta_3 - \eta_5 \cos\theta_3]\ddot{\theta}_3 + \eta_6 \sin\theta_{2s}\ddot{\theta}_{2s}$$
$$- \eta_7 \cos\theta_{2f}\ddot{\theta}_{2f} + \eta_2 \cos\theta_1 \dot{\theta}_1^2 + \eta_3 \cos\theta_2 \dot{\theta}_2^2 - [\eta_4 \cos\theta_3 + \eta_5 \sin\theta_3]\dot{\theta}_3^2$$
$$+ \eta_6 \cos\theta_{2s}\dot{\theta}_{2s}^2 + \eta_7 \sin\theta_{2f}\dot{\theta}_{2f}^2 + \lambda_1 = m_0 e\omega^2 \sin(\omega t) \tag{31}$$

$$\eta_8 \ddot{\theta}_1 + \eta_2 \left(\cos\theta_1 \ddot{x}_h + \sin\theta_1 \ddot{y}_h\right) - \eta_9 g \sin\theta_1 + \lambda_4 l \sin\theta_1 + \lambda_2 l \cos\theta_1 + \lambda_3 + \lambda_6$$
$$= 0.0043\theta_1^3 + 0.0429\theta_1^2 + 0.5052\theta_1 + 3.1455 \tag{32}$$

$$\eta_{10}\ddot{\theta}_2 - \eta_3 \cos\theta_2 \ddot{x}_h + \eta_3 \sin\theta_2 \ddot{y}_h + \eta_{11}\cos(\theta_2 - \theta_{2s})\ddot{\theta}_{2s} + \eta_{12}\sin(\theta_{2f} - \theta_2)\ddot{\theta}_{2f}$$
$$+ \eta_{11}\sin(\theta_2 - \theta_{2s})\dot{\theta}_{2s}^2 + \eta_{12}\cos(\theta_{2f} - \theta_2)\dot{\theta}_{2f}^2 + \eta_3 g \sin\theta_2 + \lambda_3 + \lambda_4 + \lambda_5$$
$$= 0.0007(\theta_2 - \theta_3)^3 - 0.0258(\theta_2 - \theta_3)^2 + 0.3236(\theta_2 - \theta_3) - 1.6792 \tag{33}$$

$$\eta_{13}\ddot{\theta}_3 + (\eta_4 \cos\theta_3 + \eta_5 \sin\theta_3)\ddot{x}_h - (\eta_4 \sin\theta_3 - \eta_5 \cos\theta_3)\ddot{y}_h - \eta_4 g \sin\theta_3$$
$$+ \eta_5 g \cos\theta_3 - 2\lambda_3 - \lambda_4 = m_0 e\omega^2 \cos\omega t \left[(c_b + y_{sp})\cos\theta_3 + x_{sp}\sin\theta_3\right]$$
$$- m_0 e\omega^2 \sin\omega t \left[(c_b + y_{sp})\sin\theta_3 - x_{sp}\cos\theta_3\right] \tag{34}$$

$$\eta_{14}\ddot{\theta}_{2s} - \eta_6 \cos\theta_{2s}\ddot{x}_h + \eta_6 \sin\theta_{2s}\ddot{y}_h + \eta_{11}\cos(\theta_2 - \theta_{2s})\ddot{\theta}_2 + \eta_{15}\sin(\theta_{2f} - \theta_{2s})\ddot{\theta}_{2f}$$
$$- \eta_{11}\sin(\theta_2 - \theta_{2s})\dot{\theta}_2^2 + \eta_{15}\dot{\theta}_{2f}^2 \cos(\theta_{2f} - \theta_{2s}) + \eta_6 g \sin\theta_{2s} - \lambda_5 =$$
$$= -0.0011(\theta_{2s} - \theta_2)^2 - 0.0029(\theta_{2s} - \theta_2) + 1.2683 \tag{35}$$

$$c_f \ddot{\theta}_{2f} - \sin\theta_{2f}\ddot{x}_h - \cos\theta_{2f}\ddot{y}_h + l_f \sin(\theta_{2f} - \theta_2)\ddot{\theta}_2 + l_s \sin(\theta_{2f} - \theta_{2s})\ddot{\theta}_{2s}$$
$$- l_t \cos(\theta_{2f} - \theta_2)\dot{\theta}_2^2 - l_s \cos(\theta_{2f} - \theta_{2s})\dot{\theta}_{2s}^2 - g \cos\theta_{2f} = 0 \tag{36}$$

The constant coefficients η_i (i=1, 2, …, 15) are defined in the Appendix. Thirteen coupled non-linear differential equations (Eqs. 24-36) for x_h, y_h, θ_1, θ_2, θ_3, θ_{2s}, θ_{2f}, λ_1, λ_2, λ_3, λ_4, λ_5, and λ_6 must be solved to analyze the dynamical behavior of the operator's body during working with a motorized backpack sprayer.

Hip and ankle joint forces in the swing phase

Forces in the human joints are important factors in the initiation and progression stages of joint diseases. Investigation of the joint forces has made it possible to prevent or minimize discomfort, fatigue, or risk of injuries. In this section, the hip and ankle joint forces in the model of the operator's body while working with a motorized backpack sprayer are calculated. Considering the upper body, Newton's second law leads to Eqs. 37

and 38.

$$\sum F_x = m_b \ddot{x}_{m_b} + m_{sp}\ddot{x}_{m_{sp}} + m_0 e\omega^2 \cos(\omega t) \tag{37}$$

$$\sum F_y = m_b \ddot{y}_{m_b} + m_{sp}\ddot{y}_{m_{sp}} + m_0 e\omega^2 \sin(\omega t) \tag{38}$$

The components of the hip joint force then become Eqs. 39 and 40.

$$F_{x_h} = m_b(\ddot{x}_h + c_b \cos\theta_3 \ddot{\theta}_3) + m_{sp}(\ddot{x}_h + x_{sp}\sin\theta_3 \ddot{\theta}_3 + (c_b + y_{sp})\cos\theta_3 \ddot{\theta}_3)$$
$$+ m_0 e\omega^2 \cos(\omega t) \tag{39}$$

$$F_{y_h} = m_b(\ddot{y}_h - c_b \sin\theta_3 \ddot{\theta}_3) + m_{sp}(\ddot{y}_h + x_{sp}\cos\theta_3 \ddot{\theta}_3 - (c_b + y_{sp})\sin\theta_3 \ddot{\theta}_3)$$
$$+ m_0 e\omega^2 \sin(\omega t) + (m_{sp} + m_b)g \tag{40}$$

Finally, the total hip joint force can be calculated using Eq. 41.

$$F_h = \sqrt{F_{x_h}^2 + F_{y_h}^2} \tag{41}$$

Considering the full body, Newton's second law leads to Eq. 42.

$$\sum F_x = m_b \ddot{x}_{m_b} + m_f \ddot{x}_{m_f} + m_h \ddot{x}_{m_h} + m_t \ddot{x}_{m_t} + m_s \ddot{x}_{m_s} + m_{sp}\ddot{x}_{m_{sp}} + m_t \ddot{x}_{m_t} + m_0 e\omega^2 \cos(\omega t) \tag{42}$$

And the x-directional force of the hip joint is expressed in Eq. 43.

$$F_{x_f} = m_b(\ddot{x}_h + c_b \cos\theta_3 \ddot{\theta}_3) + m_f(\ddot{x}_h - l_s \cos\theta_{2s}\ddot{\theta}_{2s} - l_t \cos\theta_2 \ddot{\theta}_2 - c_f \sin\theta_{2f}\ddot{\theta}_{2f})$$
$$+ m_h \ddot{x}_h + m_t(l - c_t)\cos\theta_1 \ddot{\theta}_1 + m_s(\ddot{x}_h - c_s \cos\theta_{2s}\ddot{\theta}_{2s} - l_t \cos\theta_2 \ddot{\theta}_2)$$
$$+ m_{sp}(\ddot{x}_h + x_{sp}\sin\theta_3 \ddot{\theta}_3 + (c_b + y_{sp})\cos\theta_3 \ddot{\theta}_3)$$
$$+ m_t(\ddot{x}_h - c_t \cos\theta_2 \ddot{\theta}_2) + m_0 e\omega^2 \cos(\omega t) \tag{43}$$

Considering the leg stance, the calculation of the moment about the hip joint leads to Eq. 44.

$$F_{y_f} = m_t c_t(l - c_t)\ddot{\theta}_1 + m_t g c_t \sin\theta_1 - F_{x_f} l \cos\theta_1 / l \sin\theta_1 \tag{44}$$

Finally, the total ankle joint force is calculated using Eq. 45.

$$F_f = \sqrt{F_{x_f}^2 + F_{y_f}^2} \tag{45}$$

Results and Discussion

The values of the physical parameters related to this analysis are listed in Table 1. Thirteen coupled non-linear differential equations (Eqs. 24-36) are solved in Maple software. Fig. 2 illustrates the effects of engine speed and mass of the sprayer on the hip and ankle joint forces during working with a motorized backpack sprayer.

It can be observed that the ankle force fluctuates at the beginning of the swing phase (t=[0.1-0.2]). It remains relatively constant in the middle of the swing phase t=[0.2-0.4] and again fluctuates at the end of the swing phase (t=[0.4-0.5]). The first fluctuation occurs because of the 'toe-off'. In the 'toe-off'

instance, the toe loses contact with the ground. The second fluctuation was caused by the 'heel-strike'. In this instance, there is an impact between the leg swing and the ground when the heel of the swinging leg comes into contact with the ground. The maximum force is exerted on the joints when the operator begins to swing forward ('toe-off'). Furthermore, in the instances of 'toe-off' and 'heel-strike', undesirable variations of ankle joint force F_h are noticeable. This means that ankle injuries due to vibration exposure are more likely.

Table 1- The values of physical parameters (Huang *et al.,* 2012)

Parameter	Value
Distance from hip joint to CoM of the upper body, cb	0.262 m
Distance from the ankle joint to CoM of the foot, cf	0.017 m
Distance from the knee joint to CoM of shank, cs	0.157 m
Distance from hip joint to CoM of the thigh, ct	0.192
Unbalance mass eccentricity, e	5 mm
Gravitational acceleration, g	9.81 m s^{-2}
Mass moments of inertia of sprayer about its principal axis, I_{sp}	kg.m^2
Stance leg length, l	0.700 m
Shank length, l_s	0.315 m
Thigh length, l_t	0.385 m
Unbalance mass of sprayer engine, m_o	0.01 gr
Upper body mass, m_b	26.62 kg
Foot mass, m_f	2.66 kg
Hip mass, m_h	19.97 kg
Leg mass, m_l	11.53 kg
Shank mass, m_s	3.45 kg
Sprayer mass, m_{sp}	10.50 kg
Thigh mass, m_t	8.07 kg
Sprayer position from the CoM of upper body, (x_{sp}, y_{sp})	(0.175m, 0.038m)
Engine speed, ω	3000 rpm

From a comparison between Fig. 2 (a) and (b) it is revealed that the frequency of the hip joint force increases with increased engine speed (ω). However, considerable effects on the frequency of the ankle joint force have not been observed. Additionally, with increasing the engine speed (ω), amplitudes of both the hip and ankle joint forces increase.

From a comparison between Fig. 2 (a) and (c) it can be concluded that increasing the mass of the sprayer (msp) leads to a small reduction in the oscillation of the ankle joint force. Moreover, as the mass of the sprayer (msp) increases, the magnitude of both the hip and ankle joint forces increases as well.

Fig. 3 exhibits the effect of leg length on the hip and ankle joint forces while working with a motorized backpack sprayer. It can be observed that the frequency of the hip joint force increases with decreasing the leg length l. This is because the leg stance keeps contact with the ground while the leg swings and pivots about the constrained hip like a pendulum. So, shorter operators are more vulnerable to injuries due to vibration exposure.
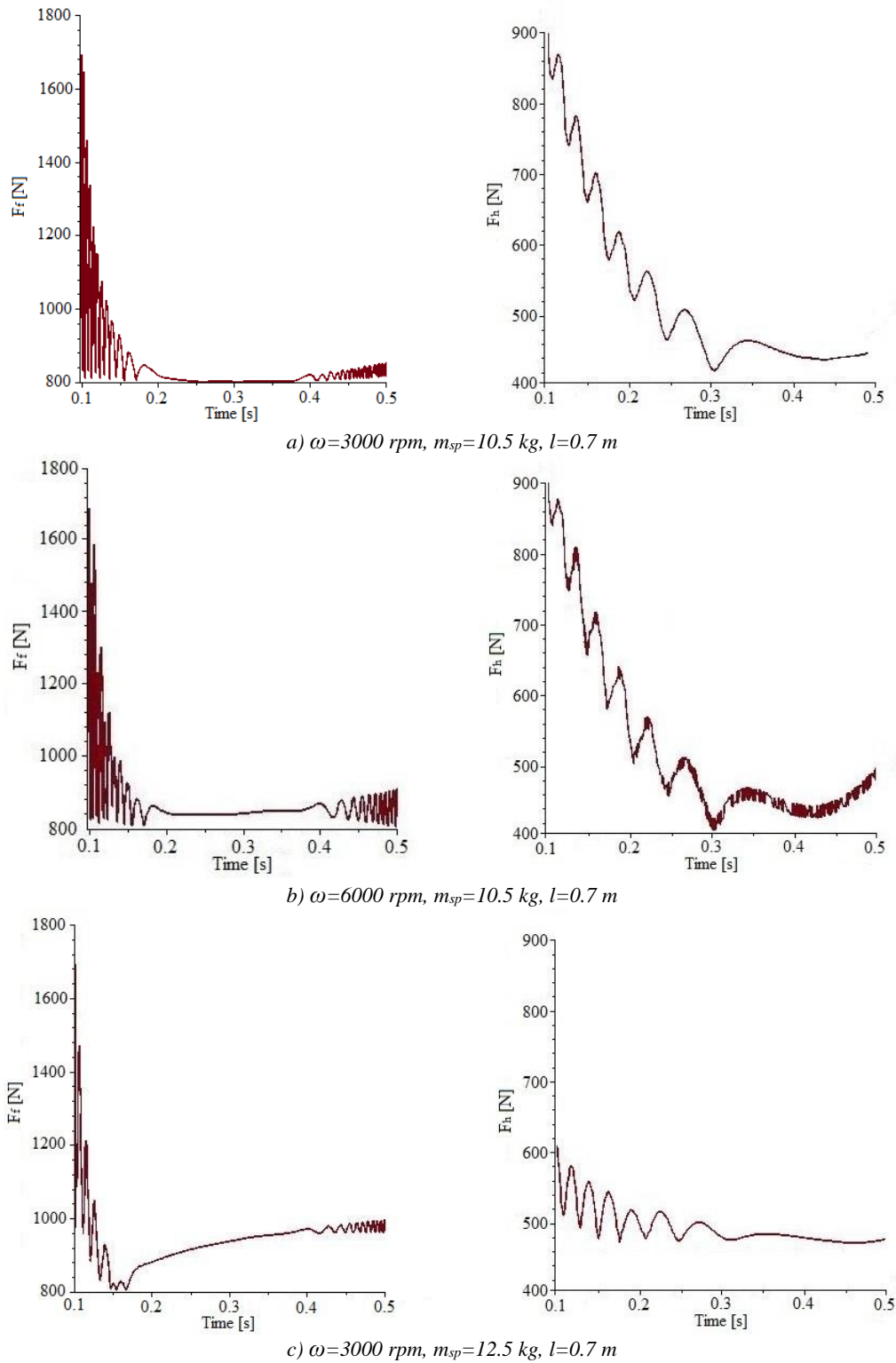
a) ω=3000 rpm, m$_{sp}$=10.5 kg, l=0.7 m

b) ω=6000 rpm, m$_{sp}$=10.5 kg, l=0.7 m

c) ω=3000 rpm, m$_{sp}$=12.5 kg, l=0.7 m

Fig.2. The hip joint force F$_h$ and ankle joint force F$_f$ for l=0.7 m and (a) m$_{sp}$=10.5 kg, ω=3000 rpm, (b) m$_{sp}$=10.5 kg, ω=6000 rpm, and (c) m$_{sp}$=12.5 kg, ω=3000 rpm

a) ω=3000 rpm, m_{sp}=10.5 kg, l=0.88 m

b) ω=3000 rpm, m_{sp}=10.5 kg, l=0.7 m

c) ω=3000 rpm, m_{sp}=10.5 kg, l=0.6 m

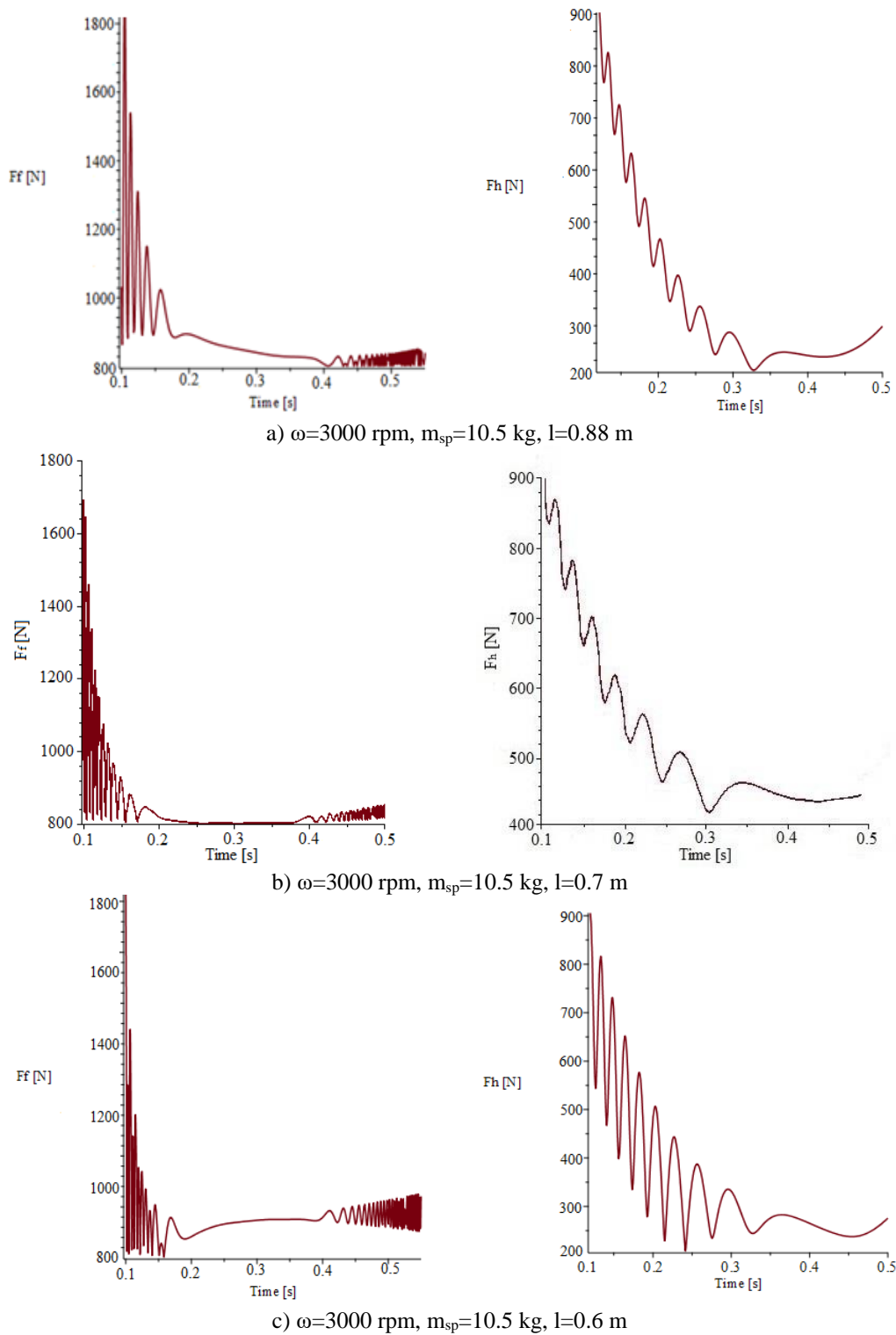**Fig.3.** The hip joint force F_h and ankle joint force F_f for m_{sp}=10.5 kg, ω=3000 rpm, and (a) l=0.7 m, (b) l=0.7 m, and (c) l=0.7 m

Conclusion

In this study, a novel assistive dynamical model for the operator's body while working with a motorized backpack sprayer was presented. In this model, the coordinate of the

sprayer relative to the body, rotational inertia of the sprayer, muscle moments acting on joints, and a kinematic coupling confining the upper body between the two legs were considered. The dynamics of the sprayer's operator were described using seven generalized coordinates. The non-linear equations of motion were obtained using the Lagrangian equations. The results obtained from the numerical analysis indicated that, at the beginning and end of the swing phase, ankle injuries due to vibration exposure are more probable. Moreover, the maximum force is exerted on the joints at the beginning of the swing phase. Furthermore, the effects of engine speed and mass of the sprayer on the hip and ankle joint forces were studied. It was found that the larger mass of the sprayer (full capacity of the tank) can lead to higher levels of joint forces and lower oscillations. The frequency of hip and ankle joint forces increased with the increase of the engine speed. The results of this paper can be used for an estimated evaluation of a patient's condition and implant design. Investigation of the effects of anthropometric specifications and sprayer position (relative to the body) on the hip and ankle joint forces while working with a motorized backpack sprayer are valuable topics for further studies.

Key Points

- Development of a seven-link dynamic model of the operator's body while working with a motorized backpack sprayer
- The non-linear differential equations of motion are formulated using Lagrangian equations and solved in Maple software
- Study of the effects of engine speed and mass of sprayer on the hip and ankle joint forces

Acknowledgments

Symbols and Abbreviations

Parameter	Description	Unite
c_b	Distance from hip joint to center of mass (CoM) of upper body	m
c_f	Distance from the ankle joint to CoM of the foot	m
c_s	Distance from the knee joint to the CoM of the shank	m
c_t	Distance from hip joint to CoM of the thigh	m
e	Unbalance mass eccentricity	mm
g	Gravitational acceleration	ms^{-2}
I_{sp}	Mass moments of inertia of sprayer about its principal axis	kg.m^2
l	Stance leg length	m
l_s	Shank length	m
l_t	Thigh length	m
m_o	Unbalance mass of sprayer engine	gr
m_b	Upper body mass	kg
m_f	Foot mass	kg
m_h	Hip mass	kg
m_l	Leg mass	kg
m_s	Shank mass	kg
m_{sp}	Sprayer mass	kg
m_t	Thigh mass	kg
(x_{sp}, y_{sp})	Sprayer position from the CoM of the upper body	(m, m)
ω	Engine speed	rpm
x_h	Horizontal coordinate of hip joint	M
y_h	Vertical coordinate of the hip joint	M
θ_1	The angle between the vertical axis and the stance leg	Radian
θ_2	The swing angle between the vertical axis and the thigh	Radian
θ_3	The angle between the vertical axis and the upper body	Radian
θ_{2s}	The swing angle between the vertical axis and the shank	Radian
θ_{2f}	The angle between the horizontal axis and the foot	Radian

Appendix

The constant coefficients for Eqs. 30-36 are as follows:

$$\eta_1 = m_h + m_l + m_t + m_b + m_{sp} + m_s + m_f \qquad \eta_2 = m_l c_l$$

$$\eta_3 = m_t c_t + m_s l_t + m_f l_t \qquad \eta_4 = m_b c_b + m_{sp}\left(c_b + y_{sp}\right)$$

$$\eta_5 = m_{sp} x_{sp} \qquad \eta_6 = m_s c_s + m_f l_s$$

$$\eta_7 = m_f c_f \qquad \eta_8 = m_l c_l^2$$

$$\eta_9 = \eta_1 l - m_l c_l \qquad \eta_{10} = m_t c_t^2 + m_s l_t^2 + m_f l_t^2$$

$$\eta_{11} = l_t \eta_6 \qquad \eta_{12} = m_f l_t c_f$$

$$\eta_{13} = I_{sp} + m_b c_b^2 + m_{sp}\left[\left(c_b + y_{sp}\right)^2 + x_{sp}^2\right] \qquad \eta_{14} = m_s c_s^2 + m_f l_s^2$$

$$\eta_{15} = m_f l_s c_f$$

References

1. Alamoudi, M., Travascio, F., Onar-Thomas, A., Eltoukhy, M., & Asfour, S. (2018). The effects of different carrying methods on locomotion stability, gait spatio-temporal parameters, and spinal stresses. *International Journal of Industrial Ergonomics*, *67*, 81-88. https://doi.org/10.1016/j.ergon.2018.04.012
2. Astephen, J. L., Deluzio, K. J., Caldwell, G. E., & Dunbar, M. J. (2008). Biomechanical changes at the hip, knee, and ankle joints during gait are associated with knee osteoarthritis severity. *Journal of Orthopaedic Research*, *26*(3), 332-341. https://doi.org/10.1002/jor.20496
3. Correa, T. A., Crossley, K. M., Kim, H. J., & Pandy, M. G. (2010). Contributions of individual muscles to hip joint contact force in normal walking. *Journal of Biomechanics*, *43*(8), 1618-1622. https://doi.org/10.1016/j.jbiomech.2010.02.008
4. D'Souza, A. F., & Garg, V. K. (1984). *Advanced dynamics: modeling and analysis*. Prentice Hall.
5. Greenwood, D. T. (1988). *Principles of dynamics* (pp. 224-226). Englewood Cliffs, NJ: Prentice-Hall.
6. Huang, Y., Wang, Q., Chen, B., Xie, G., & Wang, L. (2012). Modeling and gait selection of passivity-based seven-link bipeds with dynamic series of walking phases. *Robotica*, *30*(1), 39-51. https://doi.org/10.1017/S0263574711000397
7. Jena, S., Kumar, A., Singh, J. K., & Mani, I. (2016). Biomechanical model for energy consumption in manual load carrying on Indian farms. *International Journal of Industrial Ergonomics*, *55*, 69-76. https://doi.org/10.1017/S0263574711000397
8. Karimi Avargani, S., Maleki, A., Besharati, S., & Ebrahimi, R. (2020). Muscle moment and angle of hip, knee and ankle joints in a seven-link model of backpack sprayer operator. *Iranian Journal of Ergonomics*, *8*(3), 36-47. https://doi.org/10.30699/jergon.8.3.36
9. Kim, Y., Lee, K. M., & Koo, S. (2018). Joint moments and contact forces in the foot during walking. *Journal of biomechanics*, *74*, 79-85. https://doi.org/10.1016/j.jbiomech.2018.04.022
10. Kouchakzadeh, A., & Beigzadeh, Y. (2015). Permitted working hours with a motorised backpack sprayer. *Biosystems Engineering*, *136*, 1-7. https://doi.org/10.1016/j.biosystemseng.2015.05.005
11. Kuo, A. D. (2001). A simple model of bipedal walking predicts the preferred speed–step length relationship. *Journal of Biomechanical Engineering*, *123*(3), 264-269. https://doi.org/10.1115/1.1372322
12. Lim, H., & Park, S. (2018). Kinematics of lower limbs during walking are emulated by springy walking model with a compliantly connected, off-centered curvy foot. *Journal of*

Biomechanics, *71*, 119-126. https://doi.org/10.1016/j.jbiomech.2018.01.031

13. Liu, B. S. (2007). Backpack load positioning and walking surface slope effects on physiological responses in infantry soldiers. *International Journal of Industrial Ergonomics*, *37*(9-10), 754-760. https://doi.org/10.1016/j.ergon.2007.06.001

14. Ma, X., Xu, J., Fang, H., Lv, Y., & Zhang, X. (2022). Adaptive Neural Control for Gait Coordination of a Lower Limb Prosthesis. *International Journal of Mechanical Sciences*, *215*, 106942. https://doi.org/10.1016/j.ijmecsci.2021.106942

15. Ma, X., Xu, J., & Zhang, X. (2023). Bilateral constrained control for prosthesis walking on stochastically uneven terrain. *International Journal of Mechanical Sciences*, *239*, 107896. https://doi.org/10.1016/j.ijmecsci.2022.107896

16. Maletsky, L. P., & Hillberry, B. M. (2005). Simulating dynamic activities using a five-axis knee simulator. *Journal of Biomechanical Engineering*, *127*, 123-133. https://doi.org/10.1115/1.1846070

17. Martin, A. E., & Schmiedeler, J. P. (2014). Predicting human walking gaits with a simple planar model. *Journal of biomechanics*, *47*(6), 1416-1421. https://doi.org/10.1016/j.jbiomech.2014.01.035

18. Sharbafi, M. A., & Seyfarth, A. (2015, May). Mimicking human walking with 5-link model using HZD controller. In *2015 IEEE International Conference on Robotics and Automation (ICRA)* (pp. 6313-6319). IEEE. https://doi.org/10.1109/ICRA.2015.7140086

19. Tlalolini, D., Chevallereau, C., & Aoustin, Y. (2010). Human-like walking: Optimal motion of a bipedal robot with toe-rotation motion. *IEEE/ASME Transactions on Mechatronics*, *16*(2), 310-320. https://doi.org/10.1109/TMECH.2010.2042458

20. Walsh, G. S., Low, D. C., & Arkesteijn, M. (2018) Effect of stable and unstable load carriage on walking gait variability, dynamic stability and muscle activity of older adults. *Journal of Biomechanics*, *73*, 18-23. https://doi.org/10.1016/j.jbiomech.2018.03.018

21. Weiss, P. L., Kearney, R. E., & Hunter, I. W. (1986). Position dependence of ankle joint dynamics—I. Passive mechanics. *Journal of Biomechanics*, *19*(9), 727-735. https://doi.org/10.1016/0021-9290(86)90196-X

22. Wisse, M., Schwab, A. L., & van der Helm, F. C. (2004). Passive dynamic walking model with upper body. *Robotica*, *22*(6), 681-688. https://doi.org/10.1017/S0263574704000475

مدل‌سازی دینامیکی بار وارد بر مفاصل ران و مچ پا، هنگام کار با سم‌پاش پشتی موتوری

صدیقه کریمی آورگانی¹، علی ملکی²*، شاهین بشارتی³، رضا ابراهیمی⁴

چکیده

هدف اصلی این مقاله توسعه یک مدل دینامیک هفت لینکی از بدن اپراتور در هنگام کار با سم‌پاش کوله‌پشتی موتـوری اسـت. ایـن مـدل شـامل مختصات سم‌پاش نسبت به بدن، اینرسی چرخشی سم‌پاش، گشتاور ماهیچه‌ای وارد بر روی مفاصل و یک کوپلینگ سینماتیکی است که تعادل بـدن را بین دو پا حفظ می‌کند. توابع قید تعیین شدند و معادلات دیفرانسیل غیرخطی حرکت توسط معادلات لاگرانژ استخراج گردیدند. نتایج نشان می‌دهد کـه در ابتدا و انتهای مرحله شناوری، تغییرات نامطلوب نیروی مفصل مچ پا قابل‌توجه است. بنابراین، آسیب مچ پا به دلیل قرار گـرفتن در معـرض ارتعـاش احتمال بیشتری دارد. سپس اثرات دور موتور و جرم سم‌پاش بر نیروهای مفصل ران و مچ پا بررسی شد. نتایج نشان داد که دور موتـور و جـرم سـم‌پاش اثرات قابل‌توجهی بر نیروهای مفصل ران و مچ پا دارد و می‌تواند به‌عنوان پارامترهای کنترلی موثر مورد استفاده قرار گیرد. همچنین، نتایج آنـالیز نشـان می‌دهد که با افزایش دور موتور، فرکانس نیروی مفصل ران افزایش می‌یابد. با این حال، اثرات قابل‌توجهی بر فرکانس نیروی مفصـل مـچ پـا مشـاهده نشده است. نتایج به‌دست‌آمده از این تحقیق می‌تواند راه‌کارهایی را به محققان در برآورد ساعات کار مجاز با سم‌پاش‌های کوله‌پشـتی موتـوری، طراحـی پروتز و محاسبات نیرویی ایمپلنت‌های ران در آینده ارائه دهد.

واژه‌های کلیدی: اپراتور، ارتعاش، معادله لاگرانژ، وزن سم‌پاش

۱- دانشجوی کارشناسی ارشد گروه مهندسی مکانیک بیوسیستم، دانشکده کشاورزی، دانشگاه شهرکرد، شهرکرد، ایران

۲- دانشیار و عضو هیات علمی گروه مهندسی مکانیک بیوسیستم، دانشکده کشاورزی، دانشگاه شهرکرد، شهرکرد، ایران

۳- مربی گروه مهندسی مکانیک بیوسیستم، دانشکده کشاورزی، دانشگاه شهرکرد، شهرکرد، ایران

۴- استادیار، گروه مهندسی مکانیک، دانشکده فنی و مهندسی، دانشگاه یاسوج، یاسوج، ایران

(Email: maleki@sku.ac.ir :نویسنده مسئول -*)